Published in final edited form as:

Structure. 2018 October 02; 26(10): 1373–1383.e4. doi:10.1016/j.str.2018.07.009.

The Structure of Melanoregulin Reveals a Role for Cholesterol Recognition in the Protein's Ability to Promote Dynein Function

Ashok K. Rout[1], **Xufeng Wu**[2], **Mary R. Starich**[1], **Marie-Paule Strub**[1], **John A. Hammer**[2,#], and **Nico Tjandra**[1,†]

[1]Biochemistry and Biophysics Center, National Institutes of Health, Bethesda, MD 20892, U. S. A.

[2]Cell Biology and Physiology Center, National Heart, Lung, and Blood Institute, National Institutes of Health, Bethesda, MD 20892, U. S. A.

SUMMARY

Melanoregulin (Mreg), is a small, highly-charged, multiply-palmitoylated protein present on the membrane of melanosomes. Mreg is implicated in the transfer of melanosomes from melanocytes to keratinocytes, and in promoting the microtubule minus end-directed transport of these organelles. The possible molecular function of Mreg was identified by solving its structure using nuclear magnetic resonance (NMR) spectroscopy. Mreg contains six α-helices forming a fishhook-like fold in which positive and negative charges occupy opposite sides of the protein's surface and sandwich a putative, cholesterol recognition sequence (CRAC motif). Mreg containing a point mutation within its CRAC motif still targets to late endosomes/lysosomes, but no longer promotes their microtubule minus end-directed transport. Moreover, wild type Mreg does not promote the microtubule minus end-directed transport of late endosomes/lysosomes in cells transiently depleted of cholesterol. Finally, reversing the charge of three clustered acidic residues partially inhibits Mreg's ability to drive these organelles to microtubule minus ends.

eTOC

A key to uncovering dynein-dependent melonosome transport is the structure of Melanoregulin. Rout et. al. report that the NMR structure of Mreg contains an α-helical, fishhook-like fold in

[†]To whom correspondence should be addressed: Lead contact: Nico Tjandra, Phone: (301)-402-3029; Fax: (301)-402-3405; tjandran@nhlbi.nih.gov. [#]John A. Hammer, Phone: (301)-496-8960; Fax: (301) 402-1519; hammerj@nhlbi.nih.gov.

Author Contributions:

A.K.R., J.A.H. and N.T. conceptualized the project. A.K.R. performed all initial NMR sample preparations, experiments, and data analysis, as well as manuscript composition and preparation. M.R.S. prepared selected unlabeled and ^{15}N-labeled MregΔ32 samples, performed NMR titrations with β-chobimalt, and assisted in final manuscript preparation. M-P.S. engineered wild-type and mutant plasmids of MregΔ32. X.W. and J.A.H. carried out all aspects of the cell biological experiments. J.A.H and N.T. edited the final manuscript, and N.T. assisted in project administration.

The atomic coordinates and structure factors have been deposited in the Protein Data bank (PDB ID 6CMY), Research Collaboratory for Structural Bioinformatics, Rutgers University, New Brunswick, NJ (http://www.rcsb.org/). The chemical shifts can be accessed through the Biological Magnetic Resonance Bank (BMRB) under accession number 30101.

Declaration of Interests

The authors declare no competing interests.

which positive and negative charges occupy opposite sides of the protein's surface, sandwiching a putative CRAC motif with an essential tyrosine.

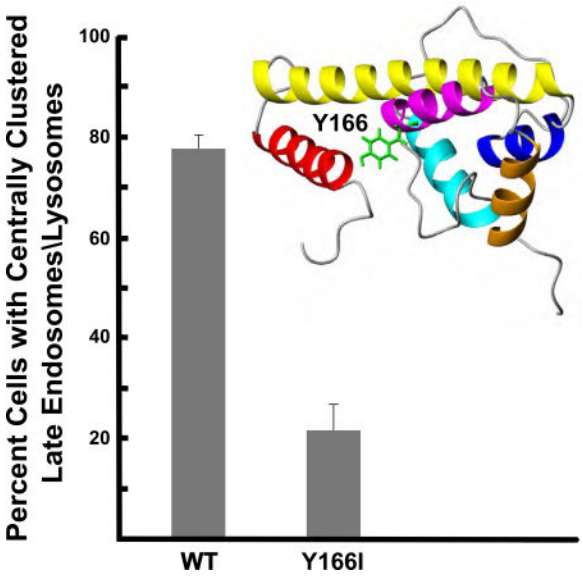

Keywords

melanoregulin; dynein; RILP; ORP1L; cholesterol; vesicular transport; NMR

INTRODUCTION

Mammalian pigmentation is driven by the formation within melanocytes of pigment-filled melanosomes and their subsequent transfer to keratinocytes, which make up the bulk of hair and skin (Kondo and Hearing, 2011; Wu and Hammer, 2014). Efficient intercellular transfer is thought to require the buildup of melanosomes at the tips of the melanocyte's long dendritic extensions, the major site of transfer. Melanosomes are accumulated at dendritic tips by a combination of long-range, bidirectional, microtubule-dependent transport within dendritic extensions and the myosin Va-dependent capture of the organelles at tips (Wu et al., 1998). Consistently, melanocytes from *dilute* mice, which lack myosin Va (Mercer et al., 1991), exhibit a dramatic redistribution of melanosomes from dendritic tips to the cell center. This redistribution leads to a reduction in intercellular melanosome transfer, resulting in a reduction or "dilution" of the mouse's coat color. For example, mice that are genetically black but also homozygous for a functional null allele at the *dilute* locus (e.g. d^{l20}) appear grey (O'Sullivan et al., 2004).

Interestingly, the coat color of *dilute* mice is restored almost completely if they are also homozygous for a mutant allele at the *dilute suppressor* (*dsu*) locus (Moore et al., 1988a; Moore et al., 1988b; O'Sullivan et al., 2004). Positional cloning revealed that this locus encodes a novel, highly-charged, vertebrate-specific protein of ~25 kDa subsequently named melanoregulin (Mreg) (O'Sullivan et al., 2004). Importantly, the large deletion identified in the mutant *dsu* allele indicated that it is the loss of expression of Mreg that rescues the loss

of expression of myosin Va (O'Sullivan et al., 2004). As expected, Mreg is highly expressed in melanocytes and resides almost exclusively on the limiting membrane of the melanosome (Ohbayashi et al., 2012; Wu et al., 2012a). The binding of Mreg to the melanosome membrane appears to be driven in large part by the addition of multiple palmitates at a cluster of six cysteines located near the protein's N-terminus, although the addition of single myristate on the sub-terminal glycine could further facilitate membrane binding (Wu et al., 2012a).

Surprisingly, *dsu* does not rescue the defect in melanosome distribution within melanocytes caused by the absence of myosin Va (O'Sullivan et al., 2004; Wu et al., 2012b). In other words, melanosomes remain congregated in the center of *dilute/dsu* melanocytes, raising the question how the coat color is rescued when the accumulation of melanosomes at dendritic tips is not restored. Resolution of this conundrum was provided by imaging the skin of *dilute* and *dilute/dsu* mice, which showed that whereas melanocytes in the skin of *dilute/dsu* mice exhibit the same central accumulation of melanosomes as seen in melanocytes in the skin of *dilute* mice, the melanosomes in the former but not the latter appear to be readily transferred to those keratinocytes that immediately surround the melanocyte's cell body (Wu et al., 2012b). This critical observation indicated how *dsu* restores coat color without restoring the defect in the intracellular distribution of melanosomes. Moreover, since *dsu* is a "loss-of-function" suppressor, this result argued that melanoregulin is a negative regulator of intercellular melanosome transfer (Wu et al., 2012b).

Interestingly, the over-expression of Mreg in melanocytes causes the hyper accumulation of melanosomes at microtubule minus ends, which coalesce at the microtubule organizing center (MTOC) located adjacent to the nucleus (Ohbayashi et al., 2012; Wu et al., 2012a). Similarly, the over-expression of Mreg in generic cell types like CV1 cells causes the robust accumulation of late endosomes and lysosomes at the MTOC (Damek-Poprawa et al., 2009; Wu et al., 2012a). These dramatic over-expression phenotypes suggest that Mreg somehow promotes the dynein-dependent, microtubule minus end-directed transport of these organelles. Based on a large body of work (Bonifacino and Neefjes, 2017; Kardon and Vale, 2009; Vallee et al., 2012), the recruitment of dynein to late endosomes, lysosomes and lysosome-related organelles like melanosomes is thought to require the Rab GTPase Rab7, a resident Rab in these compartments. Rab7 drives the recruitment of dynein by binding in a GTP-dependent fashion to the coiled-coil adaptor protein RILP (Jordens et al., 2001; Wu et al., 2005), which in turn binds to the p150 Glued subunit of dynactin, a regulatory complex associated with dynein (Johansson et al., 2007). Of note, recent paradigm shifting studies have shown that the dimeric nature of RILP and other adaptor proteins involved in dynein recruitment like BiCaudal is required for the dynein motor to move processively (McKenney et al., 2014). Finally, elegant work from the Neefjes lab has shown that Rab7 also binds the membrane-associated, cholesterol-sensing protein ORP1L (Johansson et al., 2005; Johansson and Olkkonen, 2005), which serves to transfer the Rab7-RILP-dynein motor complex to β3-spectrin present on the late endosome/lysosome surface (Johansson et al., 2007). This ORP1L-mediated transfer event is required for late endosome/lysosome-associated dynein to exhibit robust motor activity.

Importantly, Fukuda and colleagues have shown that Mreg also binds to RILP (Ohbayashi et al., 2012). This interaction should allow Mreg to recruit dynein to melanosomes, late endosomes and lysosomes and, upon over-expression, to drive their hyper-accumulation at the MTOC, as observed. Moreover, based in part on the fact that Mreg competes with Rab7 for binding to RILP, these authors argued that Mreg serves in lieu of Rab7 as the membrane anchor on melanosomes for the dynein motor complex. Although quite provocative, this conclusion appears at odds with previous studies linking Rab7 to the dynein-dependent positioning of melanosomes (Jordens et al., 2006), as well as with the phenotype of *dilute/dsu* mice (Wu et al., 2012b). Moreover, Wu and colleagues have suggested that Mreg over-expression might promote dynein motility indirectly by inducing a shift in membrane organization from liquid-disordered to liquid-ordered as a direct consequence of Mreg's multiple palmitates, which partition into and promote the formation of liquid-ordered lipid microdomains (Wu et al., 2012a). Relevant to this idea, studies have linked increases in the membrane content of cholesterol, another component of liquid-ordered microdomains, to increases in the dynein-dependent movement of late endosomes and lysosomes (Lebrand et al., 2002; Levental et al., 2010).

Here we sought to determine the three-dimensional structure of Mreg using nuclear magnetic resonance (NMR) spectroscopy. Given the evidence that Mreg promotes the dynein-dependent motility of organelles (Ohbayashi et al., 2012; Wu et al., 2012a), that it binds to RILP (Ohbayashi et al., 2012), and that the cholesterol binding protein ORP1L is required for the Rab7-RILP-dynactin/dynein-dependent motility of late endosomes and lysosomes (Johansson et al., 2005; Johansson et al., 2007; van der Kant et al., 2013a), we also sought to characterize a putative, tyrosine-based, cholesterol recognition motif (a CRAC motif) ((Epand, 2006, 2008; Epand et al., 2005; Greenwood et al., 2008; Li et al., 2001) located between residues 162 and 172 in Mreg. Specifically, the Mreg sequence LSERYLLVVDR matches exactly the CRAC consensus sequence L/V-$(X)_{1–5}$-Y-$(X)_{1–5}$-R/K. These motifs use their N-terminal hydrophobic residue (L/V) to establish hydrophobic contact with cholesterol, their central tyrosine (Y) to form hydrogen bonds and aromatic stacking with cholesterol, and their C-terminal charged residue (R/K) to stabilize the structure of the CRAC motif and orient it on the membrane. Importantly, we show that Mreg's putative CRAC motif is located near the surface of the protein and undergoes chemical or conformational exchange, suggesting that it is an interaction hotspot on Mreg. Consistently, changing the central tyrosine (Y166) in Mreg's CRAC motif to an isoleucine blocks Mreg's ability to promote the dynein-dependent motility of late endosomes and lysosomes. This and other data argue that Mreg's proposed recognition of cholesterol serves as a "switch" to allow membrane-bound Mreg to engage with the dynein motor complex. Finally, we draw several comparisons between Mreg and ORP1L regarding their roles in promoting the dynein-dependent motility, positioning, and fate of late endosomes and lysosomes.

RESULTS

Secondary Structure of Mreg

Efforts to purify full length Mreg (i.e. residues 1–214) for structure determination were severely hampered by the protein's very strong tendency to aggregate. The best NMR spectral quality, ^{15}N T_2 values, and sample stability were obtained using a construct containing Mreg residues 33 to 214. That said, even this shorter construct, referred to henceforth as MregΔ32, exhibited a relatively short half-life due to aggregation. To compensate for this, all NMR experiments were carried out at a protein concentration of 150 μM or lower, under reducing conditions, and in the presence of 5 mM L-Arginine and L-Glutamine. The two-dimensional ^{1}H-^{15}N HSQC spectrum of MregΔ32 showed a narrow chemical shift dispersion for ^{1}HN (Figure 1A), suggesting the presence of mostly helical and disordered regions. The helical nature of the protein was corroborated by far-UV Circular Dichroism spectroscopy (Figure S1A). A thermal CD scan at 220 nm showed that the protein was stable up to 35 °C, with the major conformation transition occurring at 60 °C (Figure S1B). For this reason, all NMR experiments were performed at 29 °C. In its reduced form, MregΔ32 ran on size exclusion chromatography as a monodisperse species, with a narrow distribution and a frictional coefficient corresponding to a globular protein of 29 kDa (Figure S1C), larger than the expected size of 21.3 kDa. In addition, no aggregates or higher molecular weight species were observed, arguing that MregΔ32 is monomeric and that it may have an elongated shape (Siegel and Monty, 1966).

Analysis of the three-dimensional NMR data sets yielded near complete backbone and side chain resonance assignments for MregΔ32. Specifically, ~91% of the backbone amides were assigned (Biological Magnetic Resonance Bank accession number 30101). Those amide resonances that could not be assigned (G^{33}, N^{34}, N^{35}, Y^{37}, S^{38}, S^{39}, D^{48}, E^{49}, L^{52}, W^{53}, S^{54}, M^{55}, T^{128}, K^{129}, S^{134}, T^{139}, R^{140}, Y^{166} and L^{209}) arose either from overlap or because the resonance was too broad to be detected. The calculated chemical shift index from the assigned Cα and Cβ secondary chemical shifts indicated the presence of six α-helices (α_1=65–78, α_2=85–115, α_3=118–128, α_4=140–152, α_5=165–176 and α_6=179–189). These six α-helices were also evident in the inter-proton NOE connectivity data (Figure 1B). Of note, the N-terminal (G^{33}-A^{64}) and C+terminal (Y^{190}-P^{214}) portions of MregΔ32 are disordered (Figure 1B).

Conformational Dynamics of MregΔ32

NMR backbone relaxation experiments were performed to further characterize the dynamics of MregΔ32. Backbone ^{15}N relaxation data measures millisecond to picosecond motions within a protein, thereby providing valuable information about the protein's overall and internal diffusion properties (Kay et al., 1989). The ^{15}N longitudinal (T_1) and transverse (T_2) relaxation times for MregΔ32 are shown in Figure 2A and B, respectively. Of note, the relaxation data for the loop connecting α3 to α4 could not be extracted because of spectral overlap and resonance line broadening. Residues in the N-terminal portion of MregΔ32 up to H^{57} showed low T_1 and high T_2 values, indicating that they undergo motions that are both fast and large in amplitude, consistent with a random coil structure. Similar relaxation behaviors were observed for the Cterminal residues that follow V^{196}. The average T_1 and T_2

values for MregΔ32, excluding the Nand C-terminal flexible regions, were 1.54 ± 0.14 s and 0.047 ± 0.002 s, respectively (Figure 2A and B). MregΔ32's core did not show large variations in relaxation values, consistent with a rigid structure. Of note, the average T_2 value for Mreg's core was somewhat shorter than expected for a molecule of this size, perhaps because of residual non-specific aggregation. That said, the average T_2 value based on the intensity envelope did not change significantly when the concentration of the protein was reduced to 30 μM (data not shown). Interestingly, the ratio of ^{15}N relaxation times (Figure 2C) for the six helices in MregΔ32 average to different values (44.9 ± 7.6 for α1, 47.5 ± 6.6 for α2, 40.9 ± 2.7 for α3, 44.5 ± 3.7 for α4, 47.2 ± 2.7 for α5, and 44.8 ± 2.9 for α6), with the longest helices (α2 and α5) having the highest average values. Since NH bond vectors of an α-helix are nearly parallel to the helix axis and their T_1/T_2 ratios are similar, the observed variations in the average T_1/T_2 ratios above implies that MregΔ32 diffuses anisotropically (Cornilescu et al., 2003)

MregΔ32 Adopts an Elongated α-Helical Conformation

The low working concentration of the MregΔ32 protein sample, combined with the relatively short T_2 values, resulted in a low signal to noise ratio in the acquired nuclear Overhauser effect (NOE) spectra. Moreover, Mreg's anisotropic shape resulted in missing long-range NOE contacts for some parts of the protein, even though the relaxation data showed that these segments of MregΔ32 are rigid and should be structured. To overcome these issues, we complemented the TALOS-derived dihedral angle restraints, NOE-derived distances, and generic hydrogen bonds restraints with three different sets of Paramagnetic Relaxation Enhancement (PRE) data to provide additional long range structural restraints. Spin labels (proxyl) were conjugated to three different sites in the MregΔ32 (Figure S2A), and ^1H-^{15}N RDCs of MregΔ32 were acquired in Pf1 phage (Figure S2B). The uncertainties in the PREs used were ±5–10 Å depending on the location of the spin label. The calculated twenty lowest energy MregΔ32 structures (Protein Data Bank code 6CMY) do not have any distance or dihedral angle violations greater than 0.5Å and 5°, respectively (Figure 3A). These structures show well-defined helices (α_1-α_6) with backbone r.m.s.d. values of 0.14 ± 0.07 Å, 0.26 ± 0.15 Å, 0.24 ± 0.24 Å, 0.13 ± 0.08 Å, 0.15 ± 0.09 Å, and 0.09 ± 0.05 Å, respectively. The overall backbone r.m.s.d. was 0.36 ± 0.20 Å obtained by superimposing all six helices. The calculated MregΔ32 structures were also cross-validated using N-H RDCs, resulting in an R value of 5.07 ± 0.10. The full structural statistics for the ensemble of twenty lowest energy structures are shown in Table 1.

The MregΔ32 structure adopts an elongated helical conformation in which the six helices form a unique fishhook-like fold (Figure 3B). Specifically, helices α1 and α2 form the "hook", whereas helices α3, α4, α5, and α6 pack together to form the "eye" of the fishhook (Figure 3B). Hydrophobic interactions involving residues L^{70}, Y^{71}, L^{73}, I^{74}, L^{90}, I^{94}, and L^{97} stabilize the "hook", while a hydrogen bond between the side chains of Q^{80} and S^{84} helps form the tight turn between helices α1 and α2. Interactions involving several hydrophobic residues stabilize the α3 to α6 helix bundle. The orientations of helices α_3 and α_5 are parallel to helix α_2, whereas the orientations of helices α_4 and α_6 are almost perpendicular to α_2 (Figure 3B). Finally, consistent with the NMR relaxation and chemical shift data, the N- and C-terminal segments of MregΔ32 are disordered and flexible.

The primary amino acid sequence of MregΔ32 contains many charged residues (27 K/R, 29 E/D). Interestingly, the electrostatic surface charge plot in Figure 3C shows that these positively and negatively charged residues cluster on opposite sides of the folded protein. These two "faces" of Mreg may be oriented relative to the organelle's membrane in such a way as to promote both organelle targeting and Meg's interaction with the dynein motor complex (see below and the Discussion). Of the four tryptophan residues present in MregΔ32, W^{53} in the flexible N-terminal region is fully exposed, W^{87} in helix α2 and W^{160} in the loop between helices α4 and α5 are partially exposed, and W^{108} in helix α2 is buried inside the hydrophobic core of the α3 to α6 helix bundle. Importantly, all the hydrophobic residues in the putative CRAC motif (^{162}LSERYLLVVDR^{172}), which are in the loop between helix α4 and α5, are surface exposed and surrounded by charged residues (R^{107}, E^{161}, E^{164}, R^{165}, R^{172}). It is also noteworthy that the W^{160} and Y^{166} aromatic rings are within 5A of one another and available for aromatic stacking with cholesterol.

Mreg Likely Recognizes Cholesterol Via its CRAC Motif

As discussed in the Introduction, the sequence of Mreg contains a potential, tyrosine-based, cholesterol recognition motif known as the CRAC motif (Epand, 2006, 2008; Epand et al., 2005; Greenwood et al., 2008; Li et al., 2001) centered around Y^{166} (^{162}LSERYLLVVDR^{172}). This putative Mreg CRAC motif matches exactly the CRAC consensus sequence (L/V-$(X)_{1–5}$-Y-$(X)_{1–5}$-R/K) and is highly conserved in Mreg proteins from different species (Figure S3). The structure of MregΔ32 shows that the CRAC motif residues form a contiguous surface on Mreg Δ32, and are positioned between the positive and negative surfaces of the protein (Figure 4C). In the absence of cholesterol derivatives, the residues surrounding Y^{166} in the putative CRAC motif have very low normalized ^{1}H-^{15}N HSQC peak intensities, with some being too broad to even be observed (Figure 4A, green bars). These observations suggest that this region undergoes chemical or conformational exchange. In attempts to demonstrate that Mreg binds to cholesterol via this putative CRAC motif, we titrated from 0 to 2.0 equivalents of the water-soluble synthetic cholesterol analog, β-chobimalt, against 140 μM MregΔ32 in Buffer E, acquiring ^{1}H-^{15}N HSQC NMR spectra every 0.25 equivalent (data not shown). Ascertaining binding by NMR was difficult, however, due to broadened crosspeaks for residues within the CRAC motif, and we did not observe consistent chemical shift perturbations across different MregΔ32 sample preparations. It is also noteworthy that four of the resonances in the CRAC motif range (E^{161}, L^{162}, E^{164}, Y^{166}) were absent or could not be unambiguously assigned. These residues, along with W^{160} and L^{168}, are highlighted on the structure shown in Figure 4B. Given our NMR data showing that the CRAC motif residues in MregΔ32 undergo exchange dynamics, which often signals functional importance (Butterwick and Palmer III, 2006; Hansen et al., 2009; Kroon et al., 2003; Sekhar et al., 2013), and the extensive evidence that CRAC motifs bind cholesterol ((Epand, 2006, 2008; Epand et al., 2005; Greenwood et al., 2008; Li et al., 2001), we decided to access the functional significance of Mreg's CRAC motif in live cells.

Cholesterol Recognition Controls Mreg's Ability to Promote Dynein Function

The over-expression of Mreg in generic cell types causes their late endosomes and lysosomes to cluster dramatically around the MTOC, i.e. MT minus ends (Ohbayashi et al.,

2012; Wu et al., 2012a). A clear mechanistic basis for interpreting this over-expression phenotype was provided by Fukuda and colleagues, who showed that Mreg binds the dynactin-interacting protein RILP (Ohbayashi et al., 2012), thereby connecting Mreg anchored in the late endosome/lysosome membrane via palmitoylation (Wu et al., 2012a) to the dynein motor complex. RILP also couples Rab7 anchored in the late endosome/lysosome membrane via farnesylation to the dynein motor complex. Importantly, the Rab7-RILP-dynein complex also contains the cholesterol-binding protein ORP1L, and the Rab7-RILP-dynein complex cannot transport late endosomes/lysosomes towards the MTOC without ORP1L (Johansson et al., 2005; Johansson et al., 2007; Jordens et al., 2001; Rocha et al., 2009). Given these observations, we asked if Mreg's ability to potentiate dynein function requires its ability to recognize cholesterol via its CRAC motif. To address this question, we over expressed in CV1 cells either full length, Neon-tagged, wild type (WT) Mreg or full length, Neon-tagged Mreg in which the Y at the center of its CRAC motif was changed to I (Y166I), and then visualized the distribution of late endosomes/lysosomes using the live-cell dye LysoTracker Red 18 h posttransfection (Figure 5). Of note, mutation of the central tyrosine residue in other CRAC motifs has been shown to inhibit their ability to bind cholesterol (Epand, 2008). As expected (Ohbayashi et al., 2012; Wu et al., 2012a), WT Mreg targeted to late endosomes/lysosomes and caused them to accumulate dramatically at the MTOC located in the cell center. This can be seen by comparing the intracellular distribution of red late endosomes/lysosomes in the green transfected cells in Figure 5, Panel A1-A3, to the distribution of red late endosomes/lysosomes in adjacent, un-transfected cells (cell boundaries are indicated for single, representative untransfected and transfected cells by the dotted and solid white lines, respectively). Indeed, the accumulation of late endosomes/lysosomes at the cell center/MTOC was observed in 77.7 ± 2.7 % of cell over-expressing WT Mreg, as compared to 18.1 ± 3.8 % of un-transfected cells (Figure 5E; compare WT to untransfected (UT); $p<0.001$) (please see Figure S4 for evidence based on staining for microtubules (Panels A1-A4) or γ-tubulin (Panels B1-B4) that the accumulation of late endosomes/lysosomes in the cell center corresponds to their accumulation at microtubule minus ends anchored at the MTOC; please also see Figure S5, Panels A1-A3, for higher magnification images that demonstrate the colocalization of WT Mreg with late endosomes/lysosomes). In sharp contrast to WT Mreg, only 21.7 ± 5.1 % of cells overexpressing Mreg Y116I (Figure 5, Panels B1-B3) exhibited central clustering of late endosomes/lysosomes, which was not statistically different from un-transfected cells (Figure 5E; compare Y166I to UT; N.S.), but was statistically different from WT Mreg (Figure 5E; compare Y166I to WT; $p<0.001$). Importantly, Mreg Y116I still targeted to late endosomes/lysosomes (compare the positions of the green and red signals in Figure 5, Panels B1 and B2, respectively, as well as the yellow signal in the overlaid image in Panel B3; see also the higher magnification images in Figure S5, Panels B1-B3), consistent with the fact that this mutant retains its palmitoylation sites (Wu et al., 2012a). Therefore, preventing Mreg that is targeted to late endosomes/lysosomes from binding cholesterol largely prevents it from promoting the dynein-dependent, microtubule minus end-directed transport of these organelles. These results are consistent with the idea that cholesterol recognition alters Mreg's orientation on the membrane in such a way as to allow it to interact with RILP, thereby promoting dynein-dependent organelle transport (see Discussion).

To provide additional evidence that Mreg's ability to promote the microtubule minus end-directed transport of late endosomes/lysosomes requires its ability to see cholesterol in the organelle's limiting membrane, we accessed this function in cells transiently depleted of cholesterol using methyl-β-cylcodextran (CD) (Mahammad, 2015). Figure S6, Panels A1-A4, and Supplemental Movie (left panel) show a representative example of a cell treated with carrier, which can be seen to reaccumulate its late endosomes/lysosomes at the MTOC within 30 min. In contrast, Figure S6, Panels B1-B4, and Supplemental Movie (right panel) show a representative example of a cell treated with CD, which does not reaccumulate its late endosomes/lysosomes at the MTOC within 30 min (of note, staining for microtubules showed that the restoration of the microtubule cytoskeleton was equivalent in the CD-treated and carrier-treated cells; DNS). These results provide additional support for our overall conclusion that Mreg's ability to promote the dynein-dependent, microtubule minus end-directed transport of late endosomes/lysosomes requires its ability to interact with cholesterol via its CRAC motif.

Finally, as described above, positively and negatively charged residues cluster on opposite surfaces of folded Mreg. This feature could in principle allow Mreg to bridge two surfaces of opposing charge, such as acidic phospholipid heads groups in the organelle membrane and a positively charged site on RILP. As a first pass at addressing this possibility, we reversed the charge of two surface-exposed charge clusters present on opposite sides of Meg (D177K/E180K/D181K and R140D/K141D/R143D) and assessed the ability of these two mutants to drive the central clustering of late endosomes/lysosomes. As shown in Figure 5, Panels C1-C3, the D177K/E180K/D181K mutant was significantly less effective than WT Mreg at promoting the central clustering of late endosomes/lysosomes (Panel E; compare D177K/E180K/D181K at 60.9 ± 1.9 % to WT at 77.7 ± 2.7 %; $p<0.01$). Conversely, the R140D/K141D/R143D mutant (Figure 5, Panels D1-D3) was not significantly different from WT Mreg in terms of promoting the central clustering of late endosomes/lysosomes (Panel E; compare R140D/K141D/R143D at 73.1 ± 2.2 % to WT at 77.7 ± 2.7 %; N.S.) (please see the higher magnification images in Figure S5, Panels C1-C3 and D1-D3, for additional evidence that these two Mreg mutants colocalize with late endosomes/lysosomes). We suggest that the acidic patch we targeted (D177, E180, D181) may facilitate Mreg's ability to promote dynein function by contributing to its ability to bind to RILP (see Discussion).

DISCUSSION

The transport and positioning of melanosomes with melanocytes, together with their eventual intercellular transfer to keratinocytes, drive mammalian pigmentation (Kondo and Hearing, 2011; Wu and Hammer, 2014). Mechanistic insight into these pathways has been aided greatly by the study of mouse coat color mutants, of which there are over 125. Central to our work here, characterization of melanocytes from the mouse coat color mutant *dilute*, which harbor a null mutation in myosin Va (Mercer et al., 1991), showed that this actin-based motor cooperates with the microtubule-based motors dynein and kinesin to position melanosomes for intercellular transfer (Wu et al., 1998) (although see Evans et al., 2014). Moreover, characterization of melanocytes from *dilute* mice that are mutated at the *dilute suppressor locus* (*dsu*), which encodes Mreg, showed that this melanosome-associated protein functions as a negative regulator of intercellular melanosome transfer (Wu et al.,

2012b). How Mreg accomplishes this task at the molecular level remains unclear, however. More clear is data demonstrating that Mreg over-expression promotes the dynein-dependent, microtubule minus end-directed transport of melanosomes, late endosomes, and lysosomes by recruiting the dynactin-interacting protein RILP (Ohbayashi et al., 2012; Wu et al., 2012a), although how this capability relates to the protein's role in intercellular melanosome transfer remains unclear. To facilitate a deeper molecular understanding of Mreg's proposed functions, we solved the structure of an N-terminally truncated version of Mreg - MregΔ32 - by solution NMR.

Our MregΔ32 structure revealed a unique fishhook-like fold in which the linker between helices α1 and α2 forms the bend, helix α2 forms the shank, helices α3 to α6 form the eye, and a flexible C-terminal tail following residue V^{196} completes the fishhook. The N-terminal 32 residues of Mreg, which contain its N-myristoylation and poly S-palmitoylation membrane anchor sites (Wu et al., 2012a), and which are missing in MregΔ32, most likely form a flexible, disordered segment based on the amino acid sequence that is delimited in MregΔ32 by residue H^{57}. A second striking feature of our structure is that the numerous positively charged and negatively charged residues present in Meg's primary sequence are clustered on opposite sides of the folded protein. As discussed below, these two "faces" of Mreg could be oriented relative to the organelle's membrane in such a way as to promote both organelle targeting and Meg's interaction with the dynein motor complex.

Perhaps the most interesting aspect of our results is our identification in Mreg of a tyrosine-based cholesterol recognition motif- a CRAC motif- that is sandwiched between its two oppositely charged faces. Importantly, Meg containing an inhibitory point mutation in this motif (Epand, 2008), while still able to target to late endosomes/lysosomes via it's N-terminal acylations, no longer promotes the accumulation of these organelles at microtubule minus ends. These results, and companion experiments performed in cholesterol-depleted cells, are consistent with the idea that cholesterol recognition alters Mreg's orientation on the membrane in such a way as to allow it to interact with RILP, thereby promoting dynein-dependent organelle transport. These results also suggest a fascinating parallel with the canonical pathway for dynein recruitment to late endosomes/lysosomes described in the Introduction, in which Rab7 recruits not only RILP (and hence the dynein motor complex), but also the cholesterol binding protein ORP1L, and ORP1L must be present in the complex for productive, microtubule minus end-directed organelle transport (Johansson et al., 2007; Rocha et al., 2009; van der Kant et al., 2013a).

We also found that reversing the charge of three closely-spaced acidic residues on one face of Mreg (D177K/E180K/D181K) significantly impaired its ability to promote the microtubule minus end-directed transport of late endosomes/lysosomes. Given that this version of Mreg targets properly (via its N-terminal acylations), and should be oriented on the membrane properly (via cholesterol binding), we suggest that the acidic face of Mreg points away from the membrane, and that the specific acidic cluster we mutated contributes to Mreg's interaction with RILP. Relevant to this idea, the crystal structure of Rab7 bound to the Rab7 binding domain of RILP (Wu et al., 2005) showed that positively charged residues on RILP (R^{245}, R^{255}, K^{259}, R^{298}, K^{300}, K^{304}) contribute to the stability of the complex. Moreover, Mreg competes with Rab7 for binding to RILP (Ohbayashi et al., 2012),

suggesting that their binding interfaces on RILP overlap at least partially. It seems plausible, therefore, that the D177K/E180K/D181K Mreg mutant is less effective at promoting dynein function because its charge complementarity with RILP, and hence its affinity for RILP, is reduced. Future efforts will be required to confirm this idea. Finally, whereas the basic face of Meg may contribute to its orientation on the membrane by interacting non-specifically with acidic phospholipid head groups in the organelle's membrane, the R140D/K141D/R143D mutant we tested promoted late endosome/lysosome clustering robustly. Either this specific basic patch is not crucial, or demonstrating the contribution made by the basic face to Mreg function requires a more sensitive assay.

In terms of insight into the molecular function of Mreg, the structural and functional data presented here are most relevant to Mreg's proposed role in recruiting the dynein motor complex to late endosomes, lysosomes and lysosome-related organelles like melanosomes. Taken together with previous work, (Damek-Poprawa et al., 2009; Ohbayashi et al., 2012; Wu et al., 2012a; Wu et al., 2012b), a picture emerges in which Mreg is recruited to these organelles via N-terminal acylation (with palmitoylation being dominant), is oriented properly on the organelle's surface by binding cholesterol in the membrane, and promotes the dynein-dependent, microtubule minus end-directed motility of the organelle by recruiting the dynactin-interacting protein RILP. As mentioned above, this scenario invites very interesting comparisons between Mreg and ORP1L even though they do not exhibit any sequence similarity. Most importantly, both promote the accumulation of late endosomes/lysosomes at the MTOC (i.e. at microtubule minus ends) when over-expressed, and this function requires that they can recognize cholesterol ((Rocha et al., 2009; van der Kant et al., 2013a), and data presented here). Our data are also interesting in light of previous studies showing that Mreg plays significant roles within retinal pigmented epithelial cells in melanosome biogenesis (Rachel et al., 2012), in the degradation of phagosomes containing photoreceptor outer discs (Damek-Poprawa et al., 2009), and in coordinating the association of phagosomes with LC3-containing compartments for subsequent degradation (Frost et al., 2015).

Cholesterol recognition could play several key roles in the function of both Mreg and ORP1L. First it could serve to orient them properly on the organelle membrane, i.e. in such a way as to promote downstream protein: protein interactions. Of note, our work here on Mreg provides considerable support for this idea. Second, cholesterol recognition by Mreg and ORP1L could promote the association of dynein with cholesterol-rich lipid microdomains present within the limiting membranes of endosomes and lysosomes. Relevant to this idea, studies have linked increases in lysosomal membrane cholesterol content to increases in the dynein-dependent movement of lysosomes (Bonifacino and Neefjes, 2017; Kardon and Vale, 2009). Moreover, Rai and colleagues (Rai et al., 2016) have shown that cholesterol-rich lipid microdomains present in the limiting membrane of phagosomes serve to cluster dyneins on the organelle's surface, resulting in more robust minus end-directed phagosome motility on single microtubules. Third, cholesterol recognition by Mreg and ORP1L could serve as a site of regulation. This has been demonstrated for ORP1L in a series of elegant studies from the Neefjes lab (Rocha et al., 2009; van der Kant et al., 2013a; van der Kant et al., 2013b; Wijdeven et al., 2016), which showed that ORP1L regulates in a cholesterol-sensitive fashion the tethering of late endosomes to the endoplasmic reticulum (ER) via an interaction

with the ER protein VAP (thereby controlling late endosome positioning), and the interaction of RILP with the HOPs complex (thereby controlling late endosome fate). These observations, which have now been extended to the control of autophagosome motility and fate (Wijdeven et al., 2016), provide a rich framework for future efforts to define the function of Mreg.

Contact for Reagent and Resource Sharing

Further information and requests for reagents may be directed to and will be fulfilled by the Lead Contact, Nico Tjandra (tjandran@nhlbi.nih.gov).

Experimental Model and Subject Details

Mreg Δ32 plasmid DNA's were cultured and amplified in *Escherichia coli* XL2Blue cells (Novagen) in LB at 37 °C. Recombinant proteins were overexpressed in *Escherichia coli* BL21(DE3) cells (Novagen) in minimal media at 18 °C overnight.

Method details

Protein Constructs and Sample Preparation

Mouse Mreg residues 33–214 from the *mus musculus* MREG gene (Genbank, Q6NVG5) were cloned into the bacterial protein expression vector pMAL2cx (New England BioLabs) to create a plasmid that directs the expression of Mreg residues 33–214 (referred to henceforth as MregΔ32) as a C-terminal fusion to maltose binding protein (MBP) (note that extensive efforts to express full length Mreg (i.e. residues 1–214) were unsuccessful due to pervasive protein aggregation). Isotopically-labeled (^{15}N, $^{15}N/^{13}C$, or $^{15}N/^{13}C/^{2}H$) fusion protein was produced in *E. coli* strain BL21 (DE3) by growing the bacteria in isotope-enriched M9 minimal media. $^{15}NH_4Cl$ and [^{13}C]-glucose were used as the sole sources of nitrogen and carbon, respectively, whereas deuteration was achieved by growing the cells in 99% $^{2}H_2O$ (Cambridge Isotope Laboratories). Selective ILV CH_3 labeling was achieved by growing the cells in the presence of the sodium salt versions of α-ketobutyric acid ($^{13}C4$, 98%; 3,3-D2, 98%) and α-ketoisovaleric (1,2,3,4-$^{13}C4$, 99%; 3,4',4',4'-D4, 98%) (Cambridge Isotopes), following the protocol of Tugarinov *et. al.* (Tugarinov et al., 2006). To prepare the protein, bacteria were grown at 37 °C to an OD_{600} of ~0.8, IPTG was added at a final concentration of 0.6 mM, and growth continued for ~18 h at 18 °C. The bacteria were then harvested by centrifugation, resuspended in the Lysis Buffer (50 mM Tris-HCl (pH 8.0), 100 mM NaCl, 1 mM EDTA (pH 8.0), and 1 mM DTT), and ruptured by three passes through a high-pressure homogenizer (EmulsiFlex-C3, Avestin). This lysate was then centrifuged at 17,000 rpm (34541 × g) for 30 min at 4 °C in an SS-34 rotor. The resulting supernatant was loaded onto a 22 ml amylose column (New England Biolabs) equilibrated with the Lysis Buffer, the column was washed extensively with the Lysis Buffer, and the MregΔ32 fusion protein eluted using 10 mM maltose in the Lysis Buffer. The eluted protein was exchanged into Buffer A (50 mM Tris-HCl (pH 8.0), 1 mM EDTA (pH 8.0), and 1 mM DTT) by dialysis, loaded onto a HiTrap-Q column equilibrated with Buffer A, washed extensively with Buffer A, and eluted using a salt gradient in Buffer B (50 mM Tris-HCl (pH 8.0), 1 mM EDTA (pH 8.0), 1 mM DTT, and 1 M NaCl). The fusion protein, which eluted at

~ 150 mM NaCl, was exchanged into Buffer C (50 mM Tris-HCl (pH 8.0), 100 mM NaCl, 1 mM EDTA (pH 8.0), and 1 mM DTT) by Amicon ultra-centrifugal filters (Millipore), and then incubated overnight at room temperature with $(His)_6$-tagged TEV protease (a kind gift from Dr. David S. Waugh (Kapust et al., 2001) at a ratio of 1: 100 TEV protease to fusion protein (based OD_{280}) to cleave MregΔ32 from MBP. To remove the MBP, the TEV-cleaved material was buffer exchanged to Buffer A by PD-10 desalting column and was then loaded onto a HiTrap-Q column as described above. MregΔ32 (along with the TEV protease) comes out in the flow-through, whereas the MBP binds to the column. To remove the TEV protease, the HiTrap-Q column flow-through was exchanged into Buffer D (50 mM Tris-HCl (pH 8.0) and 100 mM NaCl) and loaded onto a Ni-NTA column (Thermo Fisher Scientific) equilibrated with Buffer D. MregΔ32 comes out in the flow-through, whereas the $(His)_6$-tagged TEV protease binds to the column. The purity of MregΔ32 was assessed SDS-PAGE and its identity confirmed by liquid chromatography-mass spectrometry (Agilent 6224) ESI TOF LC-MS) (MregΔ32's measured MW of 21334.53 Da was essentially identical to its theoretical MW of 21334.12 Da). The three, single MregΔ32 cysteine variants (S60C, S136C and S198C) were prepared using a Quick-Change site-directed mutagenesis kit (Stratagene). All mutants were confirmed by DNA sequencing, and then expressed and purified using the protocol described above.

NMR Spectroscopy

Prior to performing NMR spectroscopy, purified MregΔ32 was exchanged into Buffer E (50 mM Potassium Phosphate (pH 6.3), 1 mM EDTA (pH 8.0), 1 mM DTT and 0.02% (w/v) NaN_3) by Amicon Ultra centrifugal filters (Millipore). Following buffer exchange, L-Arginine and L-Glutamine were added at final concentrations of 5 mM to improve the solubility and stability of the protein (Golovanov et al., 2004). Given that MregΔ32 tends to aggregate at high concentrations, all NMR experiments were carried out at MregΔ32 concentrations between 100 and 150 μM. NMR experiments were performed at 29 °C on a Bruker Avance 600 MHz spectrometer with a room temperature probe, and on Bruker Avance 600, 800, or 900 MHz spectrometers with cryogenic probes. The experiments used to assign backbone resonance assignments and structural restraints were performed as follows: 3D HNCO (Farrow et al., 1994), HNCA (Grzesiek and Bax, 1992b), CBCA(CO)NH (Grzesiek and Bax, 1992a), HNCACB (Wittekind and Mueller, 1993), and HBHA(CO)NH, 3D ^{15}N-edited NOESY-HSQC (τ_{mix}=80ms), and 3D ^{13}C-edited NOESY-HSQC (τ_{mix}=120ms). For a review of the conventional, 3D NMR experiments performed in this study, see Bax and Grzesiek (Bax and Grzesiek, 1993). To obtain long-range structural restraints, selective ILV-CH_3 labeling of MregΔ32 in D_2O was used for HMQC-CT, HMCMCBCA, NOESY-HHC-HMQC (τ_{mix}=250ms) and NOESY-HCC-HMQC (τ_{mix}=250ms) (Godoy-Ruiz et al., 2010; Tugarinov and Kay, 2003). The backbone ^{15}N T_1 measurement at 900 MHz proton resonance frequency and at 29 ºC was acquired using 256*1024 complex points along the t_1 and t_2 dimensions, respectively, and inversion recovery delays of 8, 128, 384, 608, 800, 1056, 1280, and 1496 ms (Barbato et al., 1992). The ^{15}N T_2 measurement was carried out with the same acquisition parameters using CPMG pulse sequence and relaxation delays of 2, 6, 12, 20, 30, 42, 56, and 70 ms (Barbato et al., 1992). All NMR data were processed using NMRPipe and analyzed with nmrDraw (Delaglio et al., 1995), PIPP (Garrett et al., 1991) and CARA (Keller, 2004). NMR

experimental errors were estimated based on the spectral noise as described previously (Farrow et al., 1994).

Paramagnetic Relaxation Enhancement

Three single MregΔ32 cysteine variants (S60C, S136C, and S198C) were used to obtain Paramagnetic Relaxation Enhancement (PRE) restraints for NMR structure determination. To achieve this, the purified MregΔ32 cysteine mutants were first incubated with 10 mM TCEP to reduce disulfide bonds, and then exchanged into Reaction Buffer (100 mM Tris-HCl (pH 8.0), 100 mM NaCl, and 1 mM EDTA (pH 8.0)) using a PD-10 desalting column. The spin probe labeling reaction was carried out overnight at room temperature by mixing the protein samples with a 20-fold molar excess of the paramagnetic probe PROXYL ((3-(2-Iodoacetamido)-Proxyl) (Toronto Research Chemicals). Removal of the excess spin probe and buffer exchange were performed using a PD-10 desalting column and Buffer E. The protein was then concentrated using an Amicon Ultra centrifugal filter, MWCO 3kD (Millipore). Spin probe labeling was confirmed by LC-MS. A reference sample was prepared by adding 5 mM ascorbic acid to the spin-labeled protein. 2D ^{1}H-^{15}N HSQC spectrums of the spin-labeled and reference samples revealed no obvious chemical shift changes, indicating that spin labeling did not disrupt the structure of MregΔ32. The PRE $^{1}H_N$-T_2 rates were determined from a two-time point (0.04 and 16ms) interleaved measurement using a transverse relaxation-optimized spectroscopy-based experiment (Iwahara et al., 2004).

Residual Dipolar Coupling

To obtain Residual Dipolar Couplings (RDCs), which are very useful for protein structure determination, refinement and validation (Bax et al., 2001; Tjandra and Bax, 1997), MregΔ32 was mixed with the weak alignment media Pf1 phage (10 mg/ml) (Hansen et al., 1998). The alignment of MregΔ32 was confirmed by measuring deuterium splitting (5–6Hz). To obtain N-H RDCs, two IPAP experiments (Ottiger et al., 1998) were set up, one on the isotropic reference sample and one on the aligned sample of MregΔ32. 2D ^{1}H-^{15}N HSQC spectra of these samples revealed no obvious chemical shift changes, indicating that Pf1 phage did not disrupt the conformation of MregΔ32.

NMR Structure Calculations

Cross peaks in NOESY spectra were identified, assigned, and the corresponding peak intensities translated into a continuous distribution of ^{1}H-^{1}H distances. The backbone dihedral angles ϕ and Ψ were calculated from the assigned backbone chemical shifts using the program TALOS (Shen and Bax, 2013; Shen et al., 2009). Generic hydrogen bond distance restraints were imposed for residues located at well-defined α-helical regions. With the above restraints, the structure of MregΔ32 was calculated using a simulated annealing protocol in which the bath temperature was cooled slowly from 3500 to 298K using the program Xplor-NIH (Schwieters et al., 2003). Three sets of PRE data were used explicitly for structure calculation and refinement by adding PROXYL tags at C60, C136 and C198 in MregΔ32. We represented the PROXYL tag by a single conformer in our structure calculation protocol (Bermejo et al., 2009). The final MregΔ32 structure calculation employed 680 short and 422 long-range NOE constraints, 64×2 hydrogen bond distance

restraints, 231 PRE restraints, and 169×2 ϕ and Ψ dihedral angle restraints. Selective Ile, Leu and Val methyl NOESY restraints (a total of 34) were imposed for further convergence of the NMR structures of MregΔ32. The structure of MregΔ32 was calculated and cross-validated using N-H RDCs. In this protocol, all experimental N-H RDCs were split into two sets: a working set (70%) and a test set (30%). The test set was back calculated using structures that had been refined using the working set, and a good correlation confirmed the validity of the calculated structure. Cross-validation was performed using Xplor-NIH (Schwieters et al., 2003). Structure figures were prepared using Pymol (The PyMOL Molecular Graphics System, Version 1.8 Schrödinger, LLC.) and MOLMOL (Koradi et al., 1996).

Probing the Interaction of MregΔ32 with Cholesterol

Identifying the interaction of a protein with cholesterol by NMR is challenging because cholesterol is insoluble in aqueous buffers. In an effort to overcome this hurdle, we utilized the water-soluble derivative of cholesterol, β-Chobimalt (Anatrace). A stock solution (2 mM) of this cholesterol derivative was prepared according to the manufacturer's instructions and directly dissolved in the NMR Buffer E. To probe the interaction between MregΔ32 and β-Chobimalt, a set of ^{1}H-^{15}N HSQC spectra were recorded for 140 μM ^{15}N-labeled MregΔ32 in the presence of increasing concentrations of the cholesterol derivative (+0.25 equivalent per titration point). The maximum molar ratio of MregΔ32 to cholesterol used was 1: 2.0.

Cell Biological Experiments

Full-length, wild type (WT) Mreg tagged with Neon at its C-terminus was created by swapping the Mreg insert in Mreg-EGFP-N1 (Wu et al., 2012a) into Neon-N1. To create full length versions of Neon-tagged Mreg containing mutations, Mreg inserts were synthesized de novo (Blue Heron Biotech) containing the following three mutations: (1) R140D, K141D, and R143D, (2) D177K, E180K, D181K, and (3) Y166I. Synthesized inserts were purified and cloned into Neon-N1. CV1 cells were grown in DMEM supplemented with 5% FBS, plated in Lab-Tek glass bottom chambers slides, and transfected with WT and mutant Mreg-Neon-N1 constructs using Lipofectamine 2000 (Invitrogen) essentially as described previously (Wu et al., 2012a). At 18 hours post transfection, cells were incubated for 20 min with 50 nM Lysotracker Red DND-99 (Molecular Probes) to stain acidic compartments (i.e. late endosomes and lysosomes), washed with PBS to remove excess dye, and fixed with 4% PFA. Samples were then imaged using a Zeiss 780 confocal microscope with standard configurations for red and green channels. Zprojections are shown. The degree to which late endosomes/lysosomes were clustered in the cell center was determined as described previously (Wu et al., 2012a). Significance was determined using the Student T test. To transiently deplete cholesterol using methyl-β-cylcodextran (CD), we took CV1 cells that had been transfected with WT Mreg 18 hours prior (i.e. cells in which late/endosomes were already accumulated at the MTOC), treated them for 120 min with 5 μg/ml nocodazole to disassemble their microtubule cytoskeletons (causing their late endosomes/lysosomes to respread) and either 10 mM CD or an equal volume of carrier, washed out the drugs with complete media containing LysoTracker and either 10 mM CD or an equal volume of carrier,

and performed time lapse imaging (30 min, 30s/frame) to access the cell's ability to reaccumulate its organelles at the MTOC as its microtubule cytoskeleton reassembles.

QUANTIFICATION AND STATISTICAL ANALYSIS

The population of cells with different late endosome/lysosomes was determined by visual inspection of cells using the Zeiss Zen 2.3 software. Total number of cells examined were 242 for untreated, 391 for wildtype, 415 for Y166I, 426 for D177K,E180K,D181K mutant, and 433 for R140D, K141D, R143D mutant cells. The cells were collected and analyzed in three different experiments. The error in the population reflect the standard of deviation of the three experiments. The *p* value, which was determined using the student T test, below 0.01 was considered to be significant.

Data and Software Availability

The atomic coordinates for the MregΔ32 have been deposited to the RCSB PDB (www.rcsb.org) with the PDB:6CMY. The NMR chemical shifts have been deposited to the BMRB with the BMRB:30101.

Supplementary Material

Refer to Web version on PubMed Central for supplementary material.

Acknowledgments

This work was supported by the Intramural Research Program of the National Institutes of Health, NHLBI. We thank Duck-Yeon Lee of the NHLBI Biochemistry Core and Dr. Grzegory Piszek of the NHLBI Biophysics Core for assistance in mass spectrometry and CD spectroscopy, respectively, Dr. Vitali Tugarinov for assistance in Ile, Leu, Val methyl specific labeling and the associated NMR experimental setups, Dr. Madeliene Strickland for her help in creating some of the molecular figures, Dr. Guillermo Bermejo for assistance in XPLOR-NIH calculation, and Dr. Richard Epand for helpful discussions regarding CRAC motifs.

References

Barbato G, Ikura M, Kay LE, Pastor RW, Bax A. Backbone dynamics of calmodulin studied by 15N relaxation using inverse detected two-dimensional NMR spectroscopy: the central helix is flexible. Biochemistry. 1992; 31:5269–5278. [PubMed: 1606151]

Bax A, Grzesiek S. Methodoligical advances in protein NMR. Accounts of Chemical Research. 1993; 26:131–138.

Bax A, Kontaxis G, Tjandra N. Dipolar couplings in macromolecular structure determination. Methods Enzymol. 2001; 339:127–174. [PubMed: 11462810]

Bermejo GA, Strub MP, Ho C, Tjandra N. Determination of the solution-bound conformation of an amino acid binding protein by NMR paramagnetic relaxation enhancement: use of a single flexible paramagnetic probe with improved estimation of its sampling space. J Am Chem Soc. 2009; 131:9532–9537. [PubMed: 19583434]

Bonifacino JS, Neefjes J. Moving and positioning the endolysosomal system. Curr Opin Cell Biol. 2017; 47:1–8. [PubMed: 28231489]

Butterwick JA, Palmer AG III. An inserted Gly residue fine tunes dynamics between mesophilic and thermophilic ribonucleases H. Protein Science. 2006; 15:2697–2707. [PubMed: 17088323]

Cornilescu CC, Bouamr F, Carter C, Tjandra N. Backbone 15N relaxation analysis of the N-terminal domain of the HTLV-I capsid protein and comparison with the capsid protein of HIV-1. Protein Science. 2003; 12:9.

Damek-Poprawa M, Diemer T, Lopes VS, Lillo C, Harper DC, Marks MS, Wu Y, Sparrow JR, Rachel RA, Williams DS, et al. Melanoregulin (MREG) modulates lysosome function in pigment epithelial cells. J Biol Chem. 2009; 284:10877–10889. [PubMed: 19240024]

Delaglio F, Grzesiek S, Vuister GW, Zhu G, Pfeifer J, Bax A. NMRPipe: a multidimensional spectral processing system based on UNIX pipes. J Biomol NMR. 1995; 6:277–293. [PubMed: 8520220]

Epand RM. Cholesterol and the interaction of proteins with membrane domains. Prog Lipid Res. 2006; 45:279–294. [PubMed: 16574236]

Epand RM. Proteins and cholesterol-rich domains. Biochim Biophys Acta. 2008; 1778:1576–1582. [PubMed: 18423371]

Epand RM, Sayer BG, Epand RF. Caveolin scaffolding region and cholesterol-rich domains in membranes. J Mol Biol. 2005; 345:339–350. [PubMed: 15571726]

Evans RD, Robinson C, Briggs DA, Tooth DJ, Ramalho JS, Cantero M, Montoliu L, Patel S, Sviderskaya EV, Hume AN. Myosin-Va and dynamic actin oppose microtubules to drive long-range organelle transport. Current Biology. 2014; 24:1743–1750. [PubMed: 25065759]

Farrow NA, Muhandiram R, Singer AU, Pascal SM, Kay CM, Gish G, Shoelson SE, Pawson T, Forman-Kay JD, Kay LE. Backbone dynamics of a free and phosphopeptide-complexed Src homology 2 domain studied by 15N NMR relaxation. Biochemistry. 1994; 33:5984–6003. [PubMed: 7514039]

Frost LS, Lopes VS, Bragin A, Reyes-Reveles J, Brancato J, Cohen A, Mitchell CH, Williams DS, Boesze-Battaglia K. The Contribution of Melanoregulin to Microtubule-Associated Protein 1 Light Chain 3 (LC3) Associated Phagocytosis in Retinal Pigment Epithelium. Molecular Neurobiology. 2015; 52:1135–1151. [PubMed: 25301234]

Garrett DS, Powers R, Gronenborn AM, Clore GM. A common sense approach to peak picking two-, three-, and four-dimensional spectra using automatic computer analysis of contour diagrams. J of Mag Res. 1991; 95:214–220.

Godoy-Ruiz R, Guo C, Tugarinov V. Alanine methyl groups as NMR probes of molecular structure and dynamics in high-molecular-weight proteins. J Am Chem Soc. 2010; 132:18340–18350. [PubMed: 21138300]

Golovanov AP, Hautbergue GM, Wilson SA, Lian LY. A simple method for improving protein solubility and long-term stability. J Am Chem Soc. 2004; 126:8933–8939. [PubMed: 15264823]

Greenwood AI, Pan J, Mills TT, Nagle JF, Epand RM, Tristram-Nagle S. CRAC motif peptide of the HIV-1 gp41 protein thins SOPC membranes and interacts with cholesterol. Biochim Biophys Acta. 2008; 1778:1120–1130. [PubMed: 18262490]

Grzesiek S, Bax A. Correlating backbone amide and side chain resonances in larger proteins by multiple relayed triple resonance NMR. J Am Chem Soc. 1992a; 14:6291–6293.

Grzesiek S, Bax A. Improved 3D triple-resonance NMR techniques applied to a 31-kDa protein. J of Mag Res. 1992b; 96:432–440.

Hansen DF, Zhou Z, Feng H, Jenkins LMM, Bai Y, Kay LE. Binding Kinetics of Histone Chaperone Chz1 and Variant Histone H2A.Z-H2B by Relaxation Dispersion NMR Spectroscopy. J Mol Biol. 2009; 387:1–9. [PubMed: 19385041]

Hansen MR, Mueller L, Pardi A. Tunable alignment of macromolecules by filamentous phage yields dipolar coupling interactions. Nat Struct Biol. 1998; 5:1065–1074. [PubMed: 9846877]

Iwahara J, Schwieters CD, Clore GM. Ensemble approach for NMR structure refinement against (1)H paramagnetic relaxation enhancement data arising from a flexible paramagnetic group attached to a macromolecule. J Am Chem Soc. 2004; 126:5879–5896. [PubMed: 15125681]

Johansson M, Lehto M, Tanhuanpaa K, Cover TL, Olkkonen VM. The oxysterol-binding protein homologue ORP1L interacts with Rab7 and alters functional properties of late endocytic compartments. Mol Biol Cell. 2005; 16:5480–5492. [PubMed: 16176980]

Johansson M, Olkkonen VM. Assays for interaction between Rab7 and oxysterol binding protein related protein 1L (ORP1L). Methods Enzymol. 2005; 403:743–758. [PubMed: 16473636]

Johansson M, Rocha N, Zwart W, Jordens I, Janssen L, Kuijl C, Olkkonen VM, Neefjes J. Activation of endosomal dynein motors by stepwise assembly of Rab7-RILP-p150Glued, ORP1L, and the receptor betalll spectrin. J Cell Biol. 2007; 176:459–471. [PubMed: 17283181]

Jordens I, Fernandez-Borja M, Marsman M, Dusseljee S, Janssen L, Calafat J, Janssen H, Wubbolts R, Neefjes J. The Rab7 effector protein RILP controls lysosomal transport by inducing the recruitment of dynein-dynactin motors. Curr Biol. 2001; 11:1680–1685. [PubMed: 11696325]

Jordens I, Westbroek W, Marsman M, Rocha N, Mommaas M, Huizing M, Lambert J, Naeyaert JM, Neefjes J. Rab7 and Rab27a control two motor protein activities involved in melanosomal transport. Pigment Cell Res. 2006; 19:412–423. [PubMed: 16965270]

Kapust RB, Tozser J, Fox JD, Anderson DE, Cherry S, Copeland TD, Waugh DS. Tobacco etch virus protease: mechanism of autolysis and rational design of stable mutants with wildtype catalytic proficiency. Protein Eng. 2001; 14:993–1000. [PubMed: 11809930]

Kardon JR, Vale RD. Regulators of the cytoplasmic dynein motor. Nat Rev Mol Cell Biol. 2009; 10:854–865. [PubMed: 19935668]

Kay LE, Torchia DA, Bax A. Backbone dynamics of proteins as studied by 15N inverse detected heteronuclear NMR spectroscopy: application to staphylococcal nuclease. Biochemistry. 1989; 28:8972–8979. [PubMed: 2690953]

Keller R. The Computer Aided Resonance Assignment Tutorial. Goldau, Switzrland: CANTINA Verlag; 2004.

Kondo T, Hearing VJ. Update on the regulation of mammalian melanocyte function and skin pigmentation. Expert Rev Dermatol. 2011; 6:97–108. [PubMed: 21572549]

Koradi R, Billeter M, Wuthrich K. MOLMOL: a program for display and analysis of macromolecular structures. J Mol Graph. 1996; 14:51–55. 29–32. [PubMed: 8744573]

Kroon GJ, Mo H, Martinez-Yamout MA, Dyson HJ, Wright PE. Changes in structure and dynamics of the Fv fragment of a catalytic antibody upon binding of inhibitor. Protein Sci. 2003; 12:1386–1394. [PubMed: 12824485]

Lebrand C, Corti M, Goodson H, Cosson P, Cavalli V, Mayran N, Faure J, Gruenberg J. Late endosome motility depends on lipids via the small GTPase Rab7. EMBO J. 2002; 21:1289–1300. [PubMed: 11889035]

Levental I, Grzybek M, Simons K. Greasing their way: lipid modifications determine protein association with membrane rafts. Biochemistry. 2010; 49:6305–6316. [PubMed: 20583817]

Li H, Yao Z, Degenhardt B, Teper G, Papadopoulos V. Cholesterol binding at the cholesterol recognition/interaction amino acid consensus (CRAC) of the peripheral-type benzodiazepine receptor and inhibition of steroidogenesis by an HIV TAT-CRAC peptide. Proc Natl Acad Sci U S A. 2001; 98:1267–1272. [PubMed: 11158628]

Mahammad SPI. Cholesterol Depletion Using Methyl-b-cyclodextrin. Methods in Membrane Lipids. 2015; 1232:91–102.

McKenney RJ, Huynh W, Tanenbaum ME, Bhabha G, Vale RD. Activation of cytoplasmic dynein motility by dynactin-cargo adapter complexes. Science. 2014; 345:337–341. [PubMed: 25035494]

Mercer JA, Seperack PK, Strobel MC, Copeland NG, Jenkins NA. Novel myosin heavy chain encoded by murine dilute coat colour locus. Nature. 1991; 349:709–713. [PubMed: 1996138]

Moore KJ, Seperack PK, Strobel MC, Swing DA, Copeland NG, Jenkins NA. Dilute suppressor dsu acts semidominantly to suppress the coat color phenotype of a deletion mutation, dl20J, of the murine dilute locus. Proc Natl Acad Sci U S A. 1988a; 85:8131–8135. [PubMed: 3141922]

Moore KJ, Swing DA, Rinchik EM, Mucenski ML, Buchberg AM, Copeland NG, Jenkins NA. The murine dilute suppressor gene dsu suppresses the coat-color phenotype of three pigment mutations that alter melanocyte morphology, d, ash and ln. Genetics. 1988b; 119:933–941. [PubMed: 3410303]

O'Sullivan TN, Wu XS, Rachel RA, Huang JD, Swing DA, Matesic LE, Hammer JA 3rd, Copeland NG, Jenkins NA. dsu functions in a MYO5A-independent pathway to suppress the coat color of dilute mice. Proc Natl Acad Sci U S A. 2004; 101:16831–16836. [PubMed: 15550542]

Ohbayashi N, Maruta Y, Ishida M, Fukuda M. Melanoregulin regulates retrograde melanosome transport through interaction with the RILP-p150Glued complex in melanocytes. J Cell Sci. 2012; 125:1508–1518. [PubMed: 22275436]

Ottiger M, Delaglio F, Bax A. Measurement of J and dipolar couplings from simplified twodimensional NMR spectra. J Mag Res. 1998; 131:373–378.

Rachel RA, Nagashima K, O'Sullivan TN, Frost LS, Stefano FP, Marigo V, Boesze-Battaglia K. Melanoregulin, product of dsu locus, links the BLOC-pathway and OA1 organelle biogenesis. PLoS One. 2012; 7:e42446. [PubMed: 22984402]

Rai A, Pathak D, Thakur S, Singh S, Dubey AK, Mallik R. Dynein clusters into lipid microdomains on phagosomes to drive rapid transport toward lysosomes. Cell. 2016; 164:722–734. [PubMed: 26853472]

Rocha N, Kuijl C, van der Kant R, Janssen L, Houben D, Janssen H, Zwart W, Neefjes J. Cholesterol sensor ORP1L contacts the ER protein VAP to control Rab7-RILP-p150 Glued and late endosome positioning. J Cell Biol. 2009; 185:1209–1225. [PubMed: 19564404]

Schwieters CD, Kuszewski JJ, Tjandra N, Clore GM. The Xplor-NIH NMR molecular structure determination package. J Mag Res. 2003; 160:65–73.

Sekhar A, Vallurupalli P, Kay LE. Defining a length scale for millisecond-timescale protein conformational exchange. Proc Natl Acad Sci U S A. 2013; 110:11391–11396. [PubMed: 23801755]

Shen Y, Bax A. Protein backbone and sidechain torsion angles predicted from NMR chemical shifts using artificial neural networks. J Biomol NMR. 2013; 56:227–241. [PubMed: 23728592]

Shen Y, Delaglio F, Cornilescu G, Bax A. TALOS+: a hybrid method for predicting protein backbone torsion angles from NMR chemical shifts. J Biomol NMR. 2009; 44:213–223. [PubMed: 19548092]

Siegel LM, Monty KJ. Determination of molecular weights and frictional ratios of proteins in impure systems by use of gel filtration and density gradient centrifugation. Application to crude preparations of sulfite and hydroxylamine reductases. Biochim Biophys Acta. 1966; 112:346–362. [PubMed: 5329026]

Tjandra N, Bax A. Direct measurement of distances and angles in biomolecules by NMR in a dilute liquid crystalline medium. Science. 1997; 278:1111–1114. [PubMed: 9353189]

Tugarinov V, Kanelis V, Kay LE. Isotope labeling strategies for the study of high-molecular-weight proteins by solution NMR spectroscopy. Nat Protoc. 2006; 1:749–754. [PubMed: 17406304]

Tugarinov V, Kay LE. Ile, Leu, and Val methyl assignments of the 723-residue malate synthase G using a new labeling strategy and novel NMR methods. J Am Chem Soc. 2003; 125:13868–13878. [PubMed: 14599227]

Vallee RB, McKenney RJ, Ori-McKenney KM. Multiple modes of cytoplasmic dynein regulation. Nat Cell Biol. 2012; 14:224–230. [PubMed: 22373868]

van der Kant R, Fish A, Janssen L, Janssen H, Krom S, Ho N, Brummelkamp T, Carette J, Rocha N, Neefjes J. Late endosomal transport and tethering are coupled processes controlled by RILP and the cholesterol sensor ORP1L. J Cell Sci. 2013a; 126:3462–3474. [PubMed: 23729732]

van der Kant R, Zondervan I, Janssen L, Neefjes J. Cholesterol-binding molecules MLN64 and ORP1L mark distinct late endosomes with transporters ABCA3 and NPC1. J Lipid Res. 2013b; 54:2153–2165. [PubMed: 23709693]

Wijdeven RH, Janssen H, Nahidiazar L, Janssen L, Jalink K, Berlin I, Neefjes J. Cholesterol and ORP1L-mediated ER contact sites control autophagosome transport and fusion with the endocytic pathway. Nat Commun. 2016; 7:11808. [PubMed: 27283760]

Wittekind M, Mueller L. HNCACB, a high-sensitivity 3D NMR experiment to correlate amide-proton and nitrogen resonances with the a- and b-carbon resonances in proteins. J Mag Res Ser B. 1993; 101:201–205.

Wu M, Wang T, Loh E, Hong W, Song H. Structural basis for recruitment of RILP by small GTPase Rab7. EMBO J. 2005; 24:1491–1501. [PubMed: 15933719]

Wu X, Bowers B, Rao K, Wei Q, Hammer JA 3rd. Visualization of melanosome dynamics within wild-type and dilute melanocytes suggests a paradigm for myosin V function In vivo. J Cell Biol. 1998; 143:1899–1918. [PubMed: 9864363]

Wu X, Hammer JA. Melanosome transfer: it is best to give and receive. Curr Opin Cell Biol. 2014; 29:1–7. [PubMed: 24662021]

Wu XS, Martina JA, Hammer JA 3rd. Melanoregulin is stably targeted to the melanosome membrane by palmitoylation. Biochem Biophys Res Commun. 2012a; 426:209–214. [PubMed: 22940130]

Wu XS, Masedunskas A, Weigert R, Copeland NG, Jenkins NA, Hammer JA. Melanoregulin regulates a shedding mechanism that drives melanosome transfer from melanocytes to keratinocytes. Proc Natl Acad Sci U S A. 2012b; 109:E2101–2109. [PubMed: 22753477]

HIGHLIGHTS

- Possible function of Melanoregulin (Mreg) identified by NMR solution structure
- Positively and negatively charged patches on Mreg sandwich a putative CRAC motif
- A Y166I point mutation in Mreg's CRAC motif no longer promotes organelle transport
- Mreg no longer promotes (-) end-directed transport in cholesterol-depleted cells

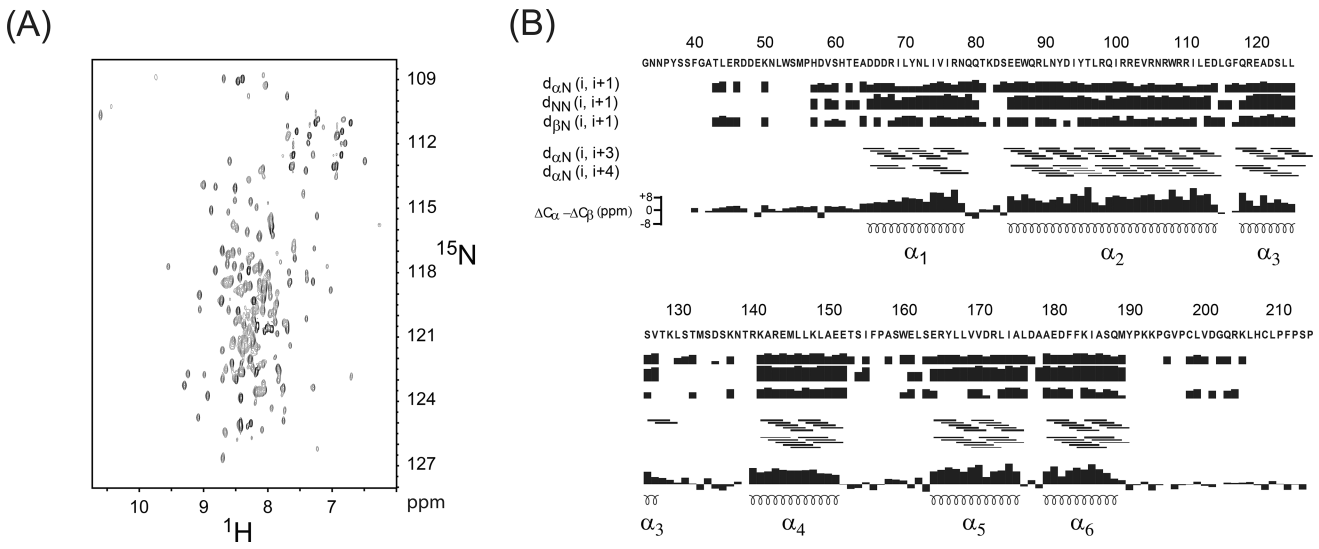

Figure 1.

Secondary structure of MregΔ32. **(A)** The ^{1}H-^{15}N HSQC NMR spectrum of MregΔ32. **(B)** The secondary chemical shift index (CSI) ΔC_α-ΔC_β defines the presence of six helices. The values of ΔC_α and ΔC_β were obtained as the differences between the experimentally observed $^{13}C_\alpha$ and $^{13}C_\beta$ chemical shifts and the corresponding random coil chemical shifts. The consecutive positive bars in the CSI plot indicate the presence of α-helical conformation of MregΔ32. The N- and C-termini do not adopt any specific secondary conformation. The defined α-helices are also confirmed by the characteristic medium range inter-proton NOE connectivity of H_α^{i} to H_β^{i+3} and strong H_N^{i} to H_N^{i+1} NOE.

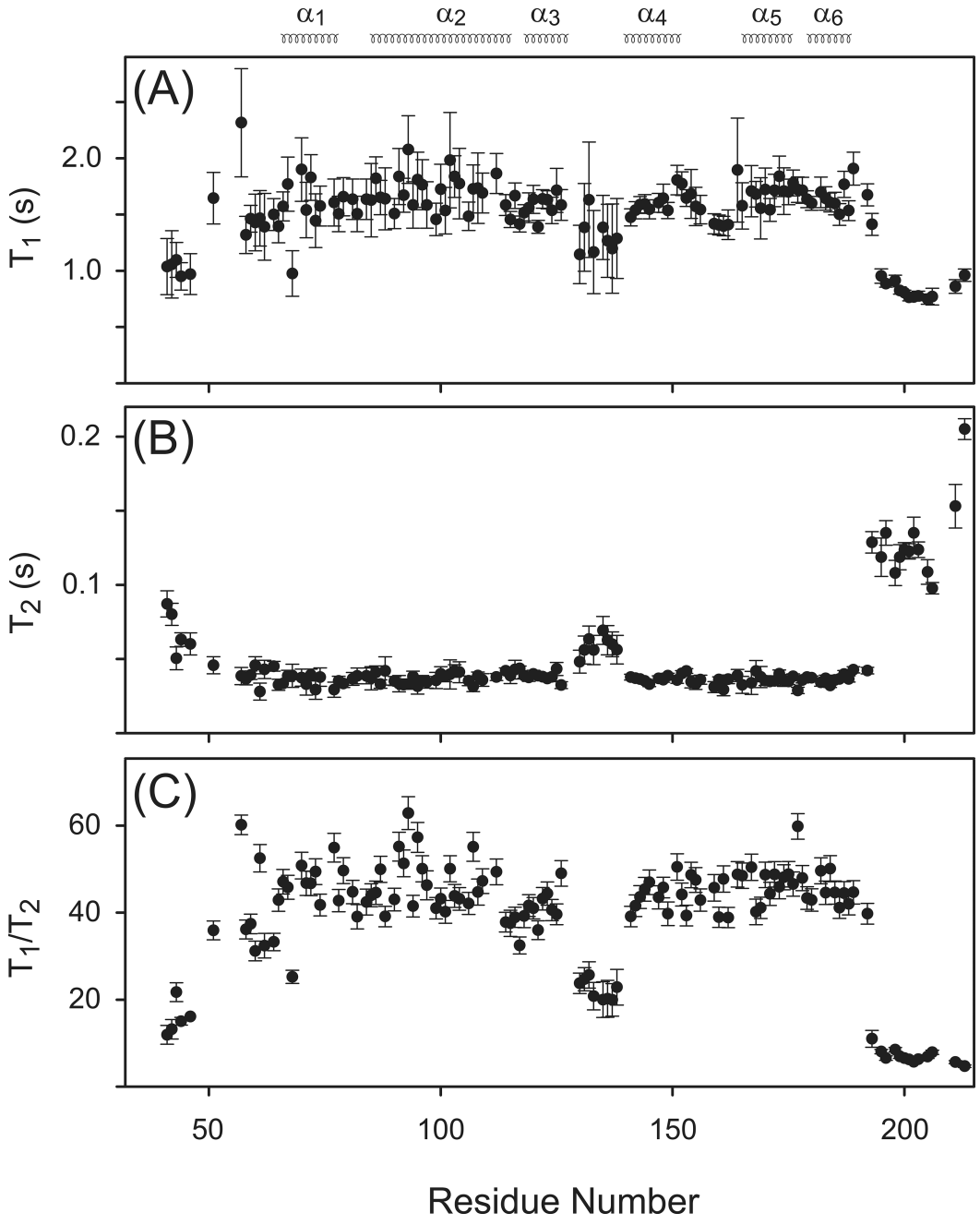

Figure 2.

Backbone ^{15}N relaxation dynamics of MregΔ32. The ^{15}N T_1 **(A)**, T_2 **(B)** relaxation data of MregΔ32 and their ratio **(C)** are plotted as a function of residue number. Relaxation values could not be estimated for those residues which are not assigned, have spectral overlap and weak intensity resulting in improper fit of their relaxation data. The mean value of T_1 and T_2 of MregΔ32 are 1.54±0.14 s and 0.047± 0.002 s respectively. The secondary structural elements are shown at the top of the Panel A.

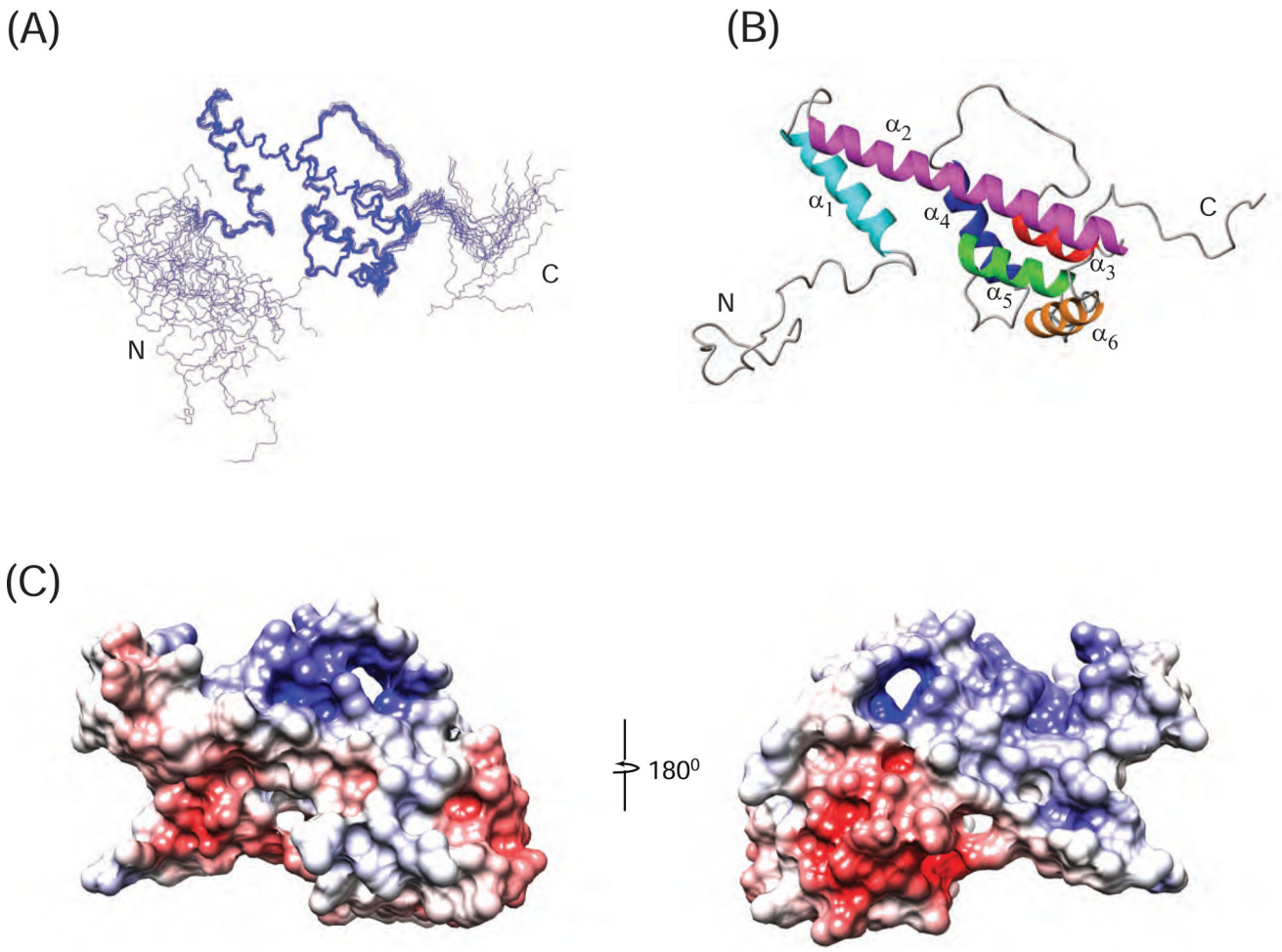

Figure 3.

NMR-derived solution structure of MregΔ32. **(A)** Superposition of an ensemble of 20 lowest energy structures of MregΔ32. **(B)** A ribbon representation of the calculated lowest energy structure of MregΔ32 showing the arrangement of the six helices which form a unique fishhook-like conformation, whereas its N- and C-termini are disordered. The helices are colored coded differently. **(C)** Electrostatic surface charge distribution of MregΔ32 in a similar orientation as in Panel B shown on the left, whereas the right panel shows an orientation 180 degree rotated from the left. For clarity, the disordered residues in the N- and C-termini have been omitted. This electrostatic map shows a polarized MregΔ32 surface with a cluster of positively and negatively charged surface occupying opposite sides of the protein.

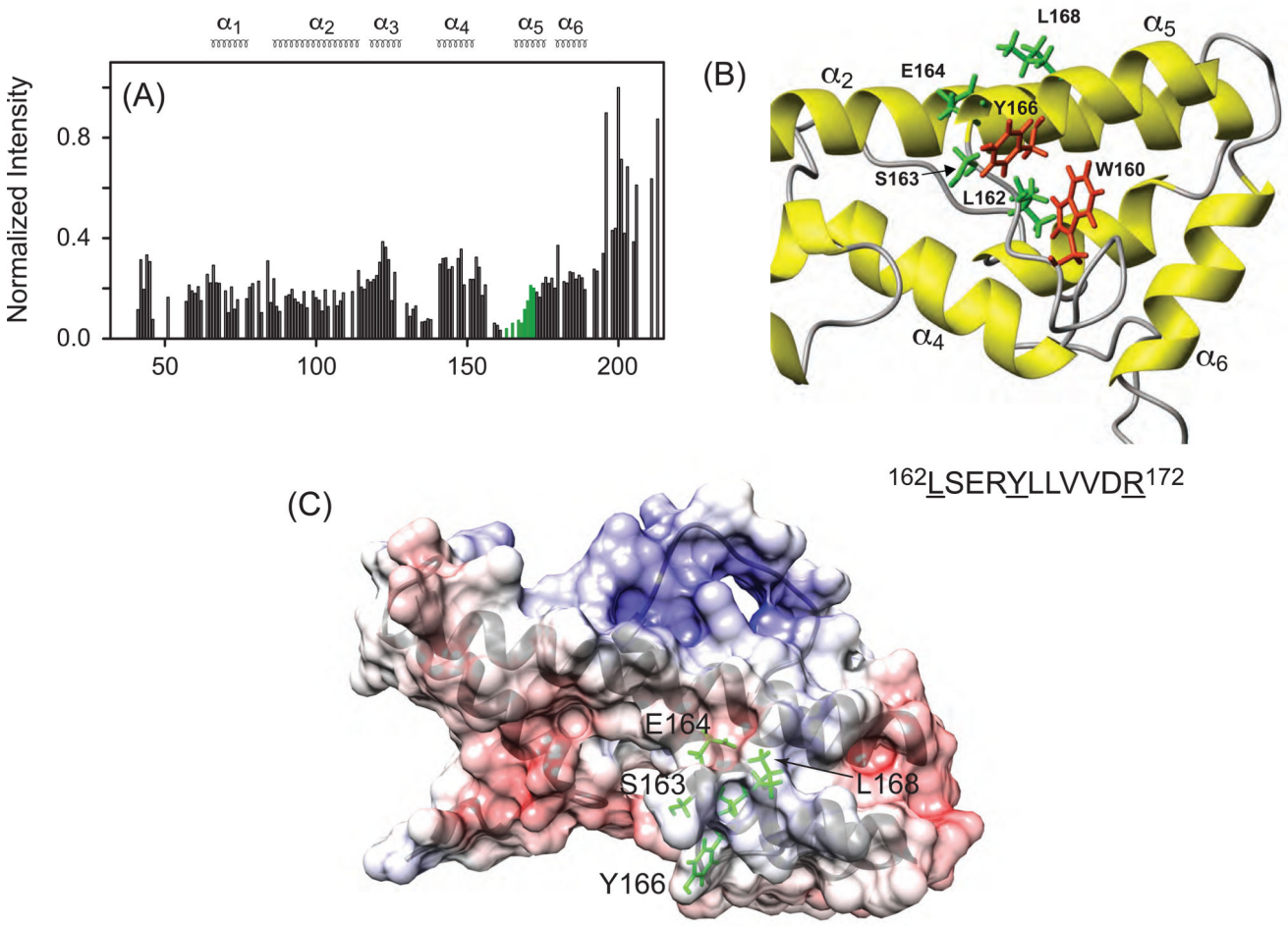

Figure 4.

Mreg's potential interaction with cholesterol. **(A)** Normalized intensities of ^{1}H-^{15}N HSQC NMR resonances for MregΔ32 plotted as a function of residue number. Note that multiple residues within the CRAC motif (residues 162–172; see green bars) have low normalized intensities. (**B**) A ribbon representation of MregΔ32 showing the position of several residues within the CRAC motif that give rise to exchange-broadened resonances. Residues L^{162}, S^{163}, E^{164} and L^{168} are shown as stick representations in green. It is noteworthy that aromatic residues W^{160} and Y^{166} (shown in red) are within 5 Å of one another and would be available for aromatic stacking with cholesterol. The MregΔ32 CRAC motif sequence is shown at the bottom of this panel. (**C**) Residues L^{162}, S^{163}, E^{164}, Y^{166} and L^{168} are shown in green and superposed on a space-filled representation of MregΔ32, where positive and negative clusters are colored in blue and red, respectively. The orientation of the molecule is the same as in Figure 3B (note that the disordered residues in the N- and C-termini have been excluded).

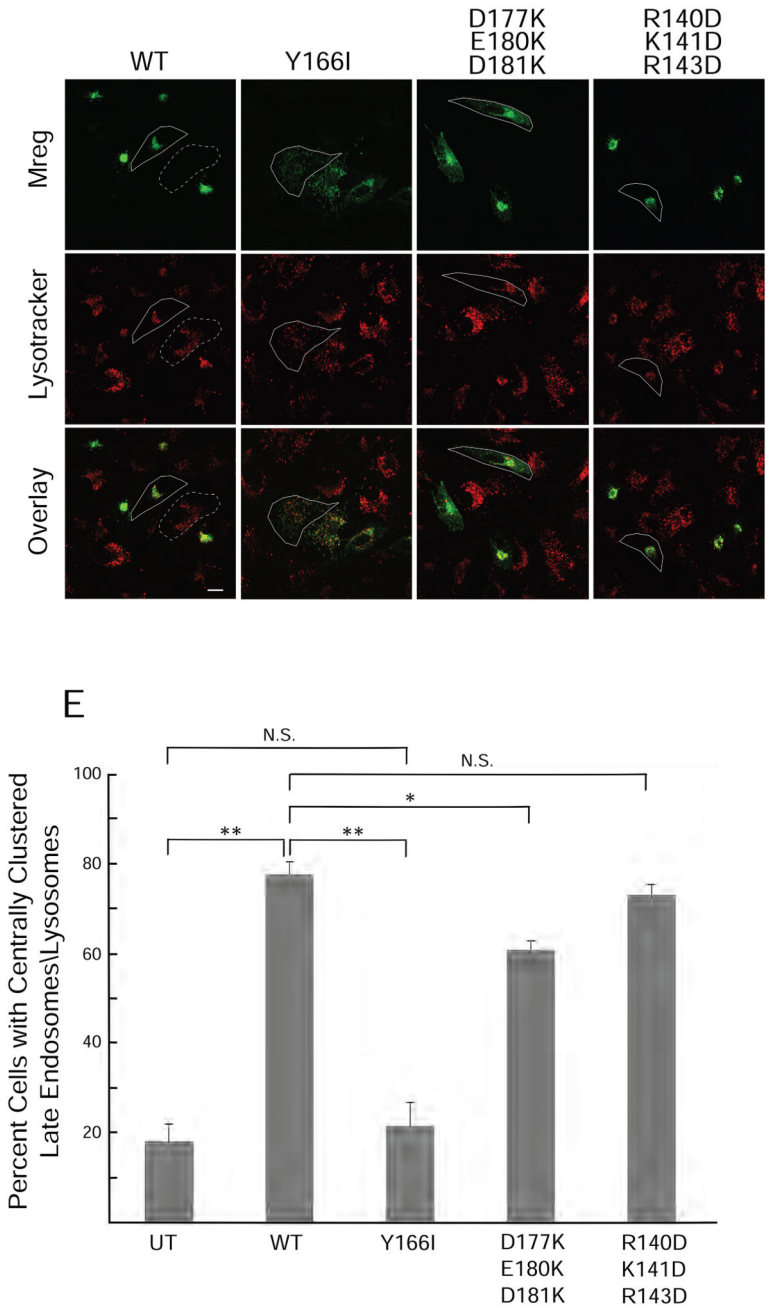

Figure 5.

(**A1–3**) Z-projection confocal image of CV1 cells transfected with Neon-tagged WT Mreg (A1) and stained 18 h post-transfection with LysoTracker Red to visualize the intracellular distribution of late endosomes and lysosomes (A2; A3 shows the overlaid image). Cell boundaries are indicated for single, representative un-transfected and transfected cells by the dotted and solid white lines, respectively. (**B1–3**) As in A1–3 except the cells were transfected with Neon-tagged Mreg containing the Y166I mutation. (**C1–3**) As in A1–3 except the cells were transfected with Neon-tagged Mreg containing the D177K, E180K, D181K mutations. (**D1–3**) As in A1–3 except the cells were transfected with Neon-tagged

Mreg containing the R140D, K141D, R143D mutations. Mag bar = 10 μm. Of note, all four constructs exhibited comparable levels of expression based on total cell fluorescence 18 h post-transfection (data not shown). (**E**) Histograms showing the percentage of cells exhibiting centrally clustered late endosomes/lysosomes. The number within each bar indicates the total number of cells analyzed for that condition. “UT” indicates un-transfected, * indicates $p< 0.01$, ** indicates $p<0.001$, and “N.S” indicates not significantly different.

Table 1

Structural statistics of an ensemble of 20 lowest energy structure of Mreg Δ32 (PDB ID: 6CMY), derived from XPLOR and PSVS 1.5.

Distance restraints (Å)		
NOE (1101)[a]		0.059 ± 0.002
Sequential NOE (|i-j| = 1) (363)		0.044 ± 0.002
Medium range NOE (2 ≤ |i-j| ≤ 5) (273)		0.048 ± 0.004
Long range NOE (|i-j| ≥ 6) (465)		0.068 ± 0.004
H-Bonds (64 × 2)		0.075 ± 0.004
Dihedral angle restraints (°)		
φ and ψ (191 × 2)		0.958 ± 0.079
Paramagnetic Relaxation Enhancement (231)		3.994 ± 0.416
Q-factor		0.217 ± 0.023
Residual Dipolar Coupling (146)		1.209 ± 0.024
R-factor		5.074 ± 0.101
D_a		−17.001 ± 0.032
R_h		0.550 ± 0.000
Deviations from idealized covalent geometry		
Bond (Å) (3132)		0.005 ± 0.000
Angle (°) (5654)		0.963 ± 0.010
Improper (°) (1624)		1.222 ± 0.011
Coordinate precision RMSD	all	ordered[b]
Backbone atoms (Å)	5.14 ± 2.07	0.36 ± 0.20
Heavy atoms (Å)	5.29 ± 2.03	1.11 ± 0.37
Ramachandran plot[b]		
Residues in most favored regions		96.8%
Residues in additional allowed regions		2.1%
Residues in generously allowed regions		1.0%
Residues in disallowed regions		0.2%

[a]Total number of restraints, residues 41–206 and

[b]Residues in regular secondary structure: 65–189